LLNL-JRNL-563754

Estimating reservoir permeabilities using the seismic response to CO2 injection and stochastic inversion

A. Ramirez, D. White, Y. Hao, K. Dyer, J. Johnson

July 10, 2012

International Journal of Greenhouse Gas Control

Disclaimer

This document was prepared as an account of work sponsored by an agency of the United States government. Neither the United States government nor Lawrence Livermore National Security, LLC, nor any of their employees makes any warranty, expressed or implied, or assumes any legal liability or responsibility for the accuracy, completeness, or usefulness of any information, apparatus, product, or process disclosed, or represents that its use would not infringe privately owned rights. Reference herein to any specific commercial product, process, or service by trade name, trademark, manufacturer, or otherwise does not necessarily constitute or imply its endorsement, recommendation, or favoring by the United States government or Lawrence Livermore National Security, LLC. The views and opinions of authors expressed herein do not necessarily state or reflect those of the United States government or Lawrence Livermore National Security, LLC, and shall not be used for advertising or product endorsement purposes.

Estimating reservoir permeabilities using the seismic response to CO_2 injection and stochastic inversion

A. Ramirez[1], D. White[2], Y. Hao[1], K. Dyer[1], and J. Johnson[3]

1-Lawrence Livermore National Laboratory
2-Geological Survey of Canada
3-Schlumberger Doll Research

LLNL-JRNL-563754

Abstract

A Markov Chain Monte Carlo (MCMC) stochastic inversion tool has been developed that identifies porosity/permeability models that minimize the misfit between observed production data, reservoir flow modeling, geostatistical methods, and a novel stochastic inversion technique to identify optimal porosity/permeability models. Reservoir model optimization is accomplished through stepwise refinement of its permeability magnitude and heterogeneity. In each step of the inversion, reservoir conditions and CO_2 migration are calculated for the current model realization under prescribed CO_2/ H_2O injection and hydrocarbon/ H_2O withdrawal. Comparison of observed seismic reflection responses with those calculated for the resultant reservoir conditions determine the associated likelihood and whether the proposed reservoir model is acceptable. This process is repeated until the process converges. The algorithm is demonstrated with a synthetic data example showing that primary features of the known porosity/ permeability distribution can be recovered. The inversion algorithm is then applied to observed seismic data example from the IEA GHG Weyburn-Midale CO_2 Monitoring and Storage Project with limited success. Shortcomings in applying the methodology to real data is assessed and recommendations for improvements are provided.

Introduction

Time-lapse 3D seismic monitoring often provides the basis for tracking the subsurface migration of CO_2 in geological storage projects (e.g., Chadwick et al., 2010; Eiken et al., 2011; Ivandic et al., 2012). A common goal in such projects is to use the monitoring data to verify the CO_2 distributions that are predicted by simulations produced for geological models of the reservoir. Typically, the CO_2 distributions that are imaged through monitoring are inconsistent with the model-based simulations to varying degrees. In such cases it is desirable to modify the geological model so that the predictions are consistent with the monitoring data. In effect, this is a more general form of history matching whereby reservoir parameters (typically permeability) are iteratively modified until the simulation results match reservoir engineering data. The addition of seismic monitoring data provides an additional constraint on the permeability distribution of the model, and in principle should improve the predictive accuracy of the model.

The process of seismic-constrained history matching is time consuming and subject to uncertainties. Ideally, a procedure is desired which automates this process and provides an assessment of the inherent non-uniqueness and uncertainties. Bayesian stochastic inversion methods are ideally suited to this purpose. Such an algorithm has been developed in this study to optimize agreement between predicted and observed storage performance, and specifically to identify optimal porosity/permeability distributions in the reservoir. Our implementation uses the Markov Chain Monte Carlo (MCMC) methodology (Mosegaard and Tarantola, 1995). 3D seismic data are utilized in conjunction with CO_2/H_2O injection and HC/H_2O production data to refine the spatial distribution of reservoir permeability, as the seismic measurements are sensitive to the CO_2 distribution that is controlled by the reservoir permeability. Existing reservoir models, geophysical logs and knowledge of the depositional environment are also used to constrain random reservoir model realizations.

In this paper we describe the inversion algorithm that has been developed, demonstrate its application on a synthetic data set, and then show initial results of applying the tool to actual seismic monitoring data from the Weyburn-Midale field. The limited success in applying the methodology to real data is assessed and recommendations for the way forward are provided.

Previous Work

Bayesian stochastic inversion has been utilized previously in a wide variety of seismic applications. In respect to reservoir characterization and monitoring, it has been used to invert seismic reflection data with well information to obtain impedance models of the subsurface, and to estimate other reservoir variables such as facies and pore fluid saturations. For example, Buland and Omre (2003), proposed a stochastic inversion of seismic amplitude vs. offset (AVO) to estimate P-wave velocity, S-wave velocity, and density. Gunning and Glinsky (2003) use a Bayesian inversion technique in conjunction with a probabilistic rock physics model to estimate a rock sorting parameter that can be a useful predictor of permeability. Eidsvik et al. (2004) integrate deterministic rock physics relations and spatial statistical representations of reservoir properties with well observations, seismic reflection times, and AVO to predict the distributions of reservoir facies and fluid saturations. Glinsky et al. (2005) suggest a Bayesian strategy to integrate seismic and geological data at various scales of resolution.

Stochastic Inversion Approach

The inverse problem under consideration can generally be described as follows. Let D denote the data space, and $\underline{x}$ denotes the model, then suppose that there exists a mapping G such that:

$$\underline{d} = G(\underline{x}) \qquad (1)$$

The goal is to find models x_0 that correspond to the set of observations, d_0. The range of possible solution models (X), is limited by a priori knowledge.

The MCMC approach that has been implemented is a derivative of the Metropolis algorithm (Metropolis et. al., 1953) as described by Mosegaard and Tarantola (1995). It uses a Markov chain process to control the sampling of the model space X. Within this framework, the solution to an inverse problem is an estimate of the posterior probability distribution defined over model space X. Then, for any potential solution $x_0 \in X$, the method will provide an estimate of the probability and confidence that state x_0 (i.e., proposed model) is the true state of the underlying system.

In this study, the models that are sought are reservoir permeability and porosity distributions. A priori knowledge consists of the locations of lithologic boundaries, lithology types, and correlations between porosity, lithology and permeability. The a priori knowledge of porosity and permeability relationships obtained from geophysical logs and core measurements provide the basis for specifying rules that govern the generation of reservoir model realizations. An MCMC simulation algorithm generates samples according to the unknown posterior distribution. The adopted Bayesian approach uses an importance-sampling algorithm based on a randomized decision rule to accept or reject the proposed models according to their consistency with the observed data.

The MCMC approach is similar to classical deterministic inversion with the random model generator replacing the deterministic updating scheme. In both cases, an initial model is chosen and responses are calculated with a forward solver. The calculated responses are compared to observed data. Finally, an updated model is chosen and the process repeats. The two approaches differ in how the updated model is chosen and the final result of the process. Specifically, MCMC produces a probability distribution defined over the model space X, whereas deterministic methods produce a single or a collection of models from X that best explain the data.

In the inversion procedure, a decision process is applied that either accepts or rejects model realizations according to their consistency with the measurements d. Specifically, for each reservoir model realization, the forward simulator is used to calculate a measurable quantity which corresponds to the observed data (in our case, seismic waveforms). These synthetic data are then compared to corresponding measurements to determine the likelihood $L(x)$ that the given state $x \in X$ produced the observed data. An accept/reject decision based upon this likelihood is used to modify the prior sampling process. The result is a new Markov chain, **R**, which samples the posterior distribution, $\mathrm{P}(x)$. These samples provide the basis for estimating the posterior distribution and any subsequent inference concerning the true unknown state of the system.

Seismic-constrained porosity/permeability inversion

Figure 1 depicts the process that has been implemented to identify reservoir models that produce CO_2 plumes that provide optimal agreement with the seismic data. Details of each step of the inversion procedure are provided in Appendix A. Uncertainties associated with both limited sensitivity and measurement error are explicitly accounted for by using the Metropolis-Hastings technique (Mosegard and Tarantola, 1995). As depicted in Figure 1, the process starts by generating an initial reservoir model realization. Then, the multi-phase/multi-component reactive transport simulator NUFT (NUFT, Nitao, 1998 a,b) is used to simulate CO_2/H_2O injection, HC/H_2O withdrawal, and CO_2 migration to a time corresponding to when the time-lapse seismic monitoring data were acquired. The corresponding seismic response is calculated for the resultant reservoir conditions using Gassmann-based fluid substitution (Gassmann, 1951) which can then be directly compared to the observed seismic response. The likelihood for each model is computed and the Metropolis-Hastings algorithm is used to decide whether the proposed model produces relatively close agreement between predicted and observed 4D seismic reflection data. Then, a new reservoir model is proposed and the process is repeated until the process converges. This approach will produce a posterior distribution that ranks all the posed reservoir models on the basis of likelihood, which is an explicit measure of consistency between predicted and observed seismic response.

The Weyburn Reservoir Model

The reservoir model used as a basis for the inversion was extracted from an existing geological model for the field that had been constructed by the Weyburn field operator (Cenovus). This model had been calibrated against injection and production data collected over a period of approximatey 50 years. The geological framework used in the inversion is shown in Figure 2. It comprises 7 lithologic layers comprising the lower Watrous Member (low permeability sandstone-mudstone) and a sequence of alternating carbonate and evaporite beds: the Ratcliffe beds, Midale evaporite, Midale Marly dolostone, Midale Vuggy limestone, and Frobisher Marly and Vuggy beds. The Midale Marly and Vuggy beds form the primary reservoir unit, but are in direct hydraulic contact with the underlying permeable Frobisher beds. Detailed descriptions of these geological units can be found in Whittaker et al. (2004). The boundaries of the individual lithologic layers in the model are defined by many well penetrations across the field and thus are considered to be very accurate. During the inversion, these layer boundaries remained fixed.

Statistical distributions of permeability/porosity for the reservoir units (Midale Marly and Vuggy) and the immediately underlying (Frobisher Marly and Vuggy) are obtained from core measurements, well log information and from the calibrated flow model. Midale formation porosity/permeability data extracted from Cenovus' model are shown in Figure 3. The histogram suggests a bimodal porosity distribution corresponding to the Vuggy limestone (mode near 0.1) and the Marly dolostone (mode centered near 0.24). A similar bimodal distribution (not shown) is also characteristic of the underlying Frobisher formation with modes centered near 0.07 and 0.24 corresponding to the Marly and Vuggy units, respectively. Porosity and permeability (Figure 3b) are correlated in both the Midale Marly and Vuggy units. The spread of permeability values (10^{-2} to 10^{3} mD) for the Vuggy limestone is generally broader than for the Marly dolostone (10^{-1} to $10^{1.5}$ mD). These porosity frequencies and porosity permeability correlations are used to govern model realizations for the inversion procedure. Permeabilities in the overlying units (Midale evaporite, Ratcliffe and lower Watrous) are set to zero, thus restricting pore fluid and pore pressure variations to the reservoir units during inversion.

Elastic properties for the various geological layers are required to calculate the associated seismic response for various reservoir realizations (see Appendix A for details). Static values of bulk density, bulk modulus and shear modulus were assigned to the Midale evaporite, Ratcliffe and lower Watrous layers. For the underlying layers, static values were assigned for the constituent matrix mineral densities and elastic moduli (see Table 1), and resultant seismic properties were calculated based on Gassmann relations for the variable pore fluid saturations and pressures that resulted from the flow simulations. Pressure effects were explicitly included for both the pore fluids and the dry rock matrix properties. An example of the dry rock matrix pressure dependence is shown in Figure 4.

Inversion results using synthetic data

To test the inversion algorithm, a synthetic data set was generated to represent a field data set for input to the inversion. Toward this end, random realizations of reservoir porosity/permeability were generated (referred to herein as "reservoir models") utilizing the geostatistical trends described earlier. One of these reservoir models was adopted as the "true" or actual model. Flow simulations were conducted which incorporated the CO_2 injection and fluid production rates that were actually used in the field. The simulation assumed that water was injected for 2 years, and that CO_2 injection started after 0.7 years of water injection. The permeability distribution for several levels within the "true" model is shown in Figure 5 along with the corresponding CO_2 distributions as determined in the flow simulations after 1.3 years of CO_2 injection.

The flow simulations determined various reservoir parameters including fluid saturations and densities and pore pressures. Seismic impedances were determined throughout the model using the calculated reservoir parameters and Gassmann's equation. Seismic reflectivity and zero-offset, 1D seismograms were subsequently calculated for the impedance model. These seismograms were adopted as the "observed data" to be used as input to the stochastic inversion. The MCMC inversion algorithm was then run to find those permeability models that best fit the seismic data. The permeabilities recovered by the inversion were then compared to the "true" model to assess their similarity.

Figure 6 shows details of the reservoir region used for the test. The region consisted of pattern 16 and included a CO_2 injector, oil producers and water injectors. The size of the region is 1.17 km by 1.17 kilometers. The reservoir models all use the same underlying lithologic designations and layer boundaries as provided in the "Cenovus model". The stochastic realizations allow porosity and permeability to vary spatially between each layer while honoring the porosity/permeability trends embedded in the Cenovus model (Figure 3).

Figures 7a and b show the permeability model as a function of MCMC iteration. The horizontal slice shown is coplanar with the CO_2 injector. The top left images shows the "true" model. Note that after 70 iterations there are substantial similarities between the recovered image and the true model. Subsequent iterations (Figure 7b) show features that are qualitatively similar to the true model; however, the inversion values are somewhat higher than those in the true model. This is not surprising because the MCMC approach searches the space of possible solutions. It moves into a region were the models are very consistent with the observations and then, can move away in order to search for other possible regions that may be consistent with the observations. This means that the best models may not necessarily be at the end of a Markov chain (i.e., last iteration number) and thus, may be found at earlier iterations.

The models that best reproduce the "observed" seismograms can be identified by examining the likelihood function values. The likelihood function (equation 10 of Appendix A) provides a metric that indicates how similar are the predicted and observed seismic data for a given reservoir model realization. The top three models, identified in this manner from a Markov chain that was 1100 iterations long, are shown in Figure 8. The left column of images shows three horizontal slices through the true permeability model, and the location of the CO_2 injector and oil producers. The remaining 3 columns of images show slices through reservoir models that exhibit the maximum likelihoods.

These maximum likelihood models are characterized by several permeability features that are observed in the true model. The slices coplanar with the CO_2 injector and oil producers (middle row of images in Figure 8) show regions of relatively high and relatively low permeabilities. Note the relatively high permeability zone located on the lower left quadrant of the true model is matched reasonably well by high permeability zones in the inversion models. The slices at 6m above the CO_2 injector (top row of images, Fig. 8) are similar to the "true" model and all show regions with relatively high permeability. Similar comments apply to the slices located 4 m below the injector well (bottom row of images).

It is well known that inversions of geophysical data are typically non-unique and the solution(s) are uncertain. One of the strengths of this stochastic inversion method is that it provides the information needed to characterize solution uncertainty. The differences between the inversion models in Figure 8 are indicative of the uncertainty associated with the inversion results. Image features that are similar in most inversion models indicate a higher level of confidence that the features represent the true model. Conversely, features that vary from one inversion to the next are associated with a higher level of uncertainty and therefore, we are less confident that they are representative of the true model.

An interesting aspect of these results is that the inverted models appear to recover reasonable permeabilities in regions not invaded by the CO_2 plume. For example, the high permeability zone in Figure 8 (middle row of images) located in the lower left quadrant of each image is not intersected by the CO_2 plume and yet the inversion recovers permeabilities that are reasonably close to the true model. In the absence of CO_2 in this zone, this result must be associated with some combination of pressure sensitivity and/or the effect of interchanging water and hydrocarbons. The permeability distribution affects the pressure field in the reservoir which in turn affects both the rock and fluid bulk moduli as incorporated in the inversion scheme. This is illustrated in Figure 9 where the differences in the calculated Vp field are shown for simulations with and without CO_2

injection and fluid production. In the first case, water was injected for 2 years with no CO_2 injection or fluid extraction allowed. This is compared to the initial test inversion case (see above) where water injection occurred for 2 years with CO_2 injection started after 0.7 years of water injection. As can be seen, significant changes in the Vp are observed between these two cases.

Inversions using real field data

The stochastic inversion was applied to the actual P-wave seismic data from the Weyburn field, for the same field pattern as used for the synthetic test described above. An example of the observed seismic data is shown in Figure 10. The flow simulation included water injection for 2 years with CO_2 injection starting after 0.7 years of water injection. For comparison with the 2001 seismic data, which were acquired 16 months after the start of CO_2 injection in the pattern, the flow simulation results corresponding to 1.3 years of CO_2 injection were used. Figure 11 shows a high likelihood model (i.e., one that minimizes the seismic misfit) from iteration 5751 of the MCMC inversion. The standard deviations in the Marly and Vuggy layers range from ~4 to 18 md and 6 to 24 md, respectively. The mean permeabilities and associated standard deviations for an ensemble of high likelihood models is shown in Figure 12.

As can be seen in Figure 13, the inversion procedure led to a reduction in the misfit between the predicted and observed seismic waveforms, but the misfit reductions were substantially less than expected. Visual inspection of the predicted and observed seismic waveforms showed relatively large differences. It would appear that the poor match between observed and synthetic waveforms fit probably affected the accuracy of the inverted porosity/permeability fields. A comparison of histograms of permeability and porosity for the optimal inversion models and the a priori porosity/permeability histograms showed great similarity. This suggests that the seismic data had limited influence in determining the posterior permeability distributions. Obviously, this is counter to the objective of applying the inversion procedure. The underlying causes of this behavior and potential means of improving the performance of the inversion scheme are discussed further below.

Computational Expense

The stochastic inversion approach implemented in this study is computationally intensive. The vast majority of computational effort is associated with execution of the flow simulator in each iteration, combined with the large number of iterations required for the Markov chains to reach convergence, typically in the range 104 – 105 iterations. The initial implementation of the inversion algorithm required between 16 and 48 days of wall clock time to reach convergence for the single reservoir pattern used in this study, when run on a 112-processor cluster. For inversion of data from the larger area monitored in the Weyburn field (19 patterns), the required time would increase substantially. Clearly, these run times needed to be reduced substantially to make the technique useful.

Changes to the initial inversion algorithm eventually improved the computational efficiency so that execution times were reduced by an order of magnitude and the time required to reach convergence was only a few days. Modifications included various multi-threading approaches. Figure 14 schematically shows the nested, parallel-thread approaches that were implemented. Each Markov chain runs on a separate thread (left side of Figure 14), with each Markov chain thread sub-divided by creating multiple reservoir realizations. Each realization is created by perturbing the last model accepted by the MCMC algorithm and is run on a separate thread (middle diagram in Figure 14). All these threads are further subdivided when the flow simulator is used because it runs in parallel mode. The combined effect of these modifications produced an improvement in performance by a factor of ~8.

Discussion

The results presented her suggest that it is possible to invert for permeability models that are consistent with seismic reflection monitoring data in a reservoir subjected to injection of super-critical CO_2. In principle, the seismic monitoring data should provide constraints on the permeability models as the seismic impedances are strongly affected by the presence of CO_2 whose distribution is controlled by the permeability field of the reservoir. In the synthetic test case, permeability models that were reasonably close to the "true" model were recovered. This is not surprising given that the synthetic seismic generated for the "true" model and adopted as the "observed" data were adherent to all of the assumptions underlying the inversion procedure. However, in applying the inversion procedure to actual seismic monitoring data from the Weyburn field, the inversion results were generally unsatisfactory. Although the misfit between the observed and calculated seismic data improved during the course of the inversion, the misfit reduction was limited and the seismic data had less affect on the resultant permeability distributions than expected.

The root cause of the poor performance of the inversion as applied to the real data is primarily due to the large initial misfit between the observed and calculated seismic data. This large misfit results from the use of constant seismic parameters (bulk and shear modulus) for the individual geological layers which don't account for observed lateral heterogeneity. As a result, the calculated seismic waveforms differed substantially from the average observed waveforms prior to any CO2 injection. The associated differences in the waveforms are large when compared to the changes induced by CO2 injection. Thus, the inversion process sought to minimize the seismic misfit using only changes in the pore fluid saturations and reservoir pressure changes, when in fact the bulk of the misfit was due to the inaccuracies in the original rock matrix properties. The latter generally have a larger influence on the seismic response than changes in the pore fluids. It is clear that the starting reservoir rock matrix seismic properties need to be more accurate for the inversion to succeed.

To mitigate the effect that inaccuracies in the starting reservoir model properties have on the inversion, a number of approaches were applied or considered. First, the rock matrix moduli for the individual layers were manually adjusted to achieve a better fit between the observed and calculated baseline data. It was clear that the elastic moduli determined from core samples were not entirely appropriate for application at the scale of the seismic data. In particular, a prominent feature of the synthetic waveforms was a peak associated with the Midale Vuggy layer that was more generally much more prominent than in the observed data. The bulk and shear moduli for this layer were reduced to provide a better initial match to the observed data. A similar observation regarding the reservoir moduli was made by Verdon et al. (201x) in geomechanical modeling. This modification improved matters, but did not entirely solve the problem.

In subsequent work, there are several other approaches that may be considered to address the effects of inaccurate elastic properties of the starting model. These include: 1) stochastic inversion for the pre-injection rock matrix seismic parameters to match the baseline data prior to the start of inversion for pore fluid effects; 2) Comparison of the difference data (i.e., monitor minus baseline) in the stochastic inversion to reduce the effects of inaccuracies in the baseline model; 3) Seismic impedances determined directly from the baseline data could be used to improve the baseline model.

Summary and Conclusions

An MCMC stochastic inversion algorithm has been developed that uses seismic reflection data to constrain reservoir permeability and porosity distributions during the injection of CO_2. The algorithm has been successfully demonstrated on a synthetic test case, where all of the assumptions underlying the inversion approach are met. The MCMC stochastic inversion identified models of reservoir porosity and permeability that best fit the “observed” seismic data and have features that are characteristic of the true porosity-permeability model. It is also possible to estimate permeability in reservoir regions that do not contain CO_2. This results from the pressure-dependance of the bulk and shear moduli.

Application of the inversion algorithm to real data from the Weyburn field was only partially successful. Inversions of the real seismic data resulted in reduction of the misfit between the predicted and observed waveforms, but the misfit improvements were less than expected. The underlying cause of this limited success was the inaccuracy of the elastic moduli used in the underlying geological model. Misfits between the observed and calculated seismic data associated with this issue, are generally larger than those produced by the injection of CO2. Thus, the inversion inappropriately attempts to eliminate these large waveform misfits through pore fluid and pressure changes. For the inversion to succeed, the strong influence of the baseline model must be mitigated either by improving the initial elastic model parameter distribution (e.g., through stochastic or conventional impedance inversion of the baseline data), or by directly utilizing the difference data (i.e., monitor minus baseline) rather than comparing the monitor data directly in the inversion process.

Computational expense remains a challenge to the general application of this algorithm. As currently implemented, the inversions required up to 9 days of computer time when running on a cluster of 112 processor cores. This was for a relatively small model.

Acknowledgements

We are grateful for the funding support provided by the Petroleum Technology Research Center, Saskatchewan, Canada. We are also grateful for the data provided by Barbara Dietiker (Geological Survey of Canada) and Erik Nickel (Saskatchewan Ministry of Energy and Resources). We also want to acknowledge the contributions of colleague Jeff Wagoner (LLNL) who provided various adaptions of the reservoir model originally developed by Cenovus. This work has been performed under the auspices of the U.S. Department of Energy by Lawrence Livermore National Laboratory under Contract DE-AC52-07NA27344.

References

Batzle, M. and Z. Wang, 1992, Seismic properties of fluids, *Geophysics*, v. 57, no. 11, pp 1396-1408.

Brown, L. 2002, *Integration of rock physics and reservoir simulation for the interpretation of time-lapse seismic data at Weyburn Field, Saskatchewan*, M. Sc. thesis, Colorado School of Mines, Golden, CO.

Buland, A., and Omre, H., 2003, Bayesian linearized AVO inversion, Geophysics January 2003 v. 68 no. 1, p. 185 – 198, doi: 10.1190/ 1.1543206.

Buscheck T., Glascoe L., Lee K., Gansemer J, Sun Y, Mansoor K, 2003, Validation of the Multiscale Thermohydrologic Model used for analysis of a proposed repository at Yucca Mountain. *J. Contaminant Hydrology*, vol. 62 no. 3, p. 421-440.

Chadwick, A., Williams, G., Delepine, N., Clochard, V., Labat, K., Sturton, S., Buddensiek, M.-L., Dillen, M., Nickel, M., Lima, A.L., Arts, R., Neele, F., Rossi, G., 2010. Quantitative analysis of time-lapse seismic monitoring data at the Sleipner CO 2 storage operation, Leading Edge, 29, 170-177.

Chen, Z, Huan, G, Ma, Y, 2006, Computational methods for multiphase flows in porous media**.** Philadelphia: Society for Industrial and Applied Mathematics, 531 p.

Eidsvik, J., Avseth, P., Omre, H., Mukerji, T., and Mavko, G., 2004, Seismic reservoir characterization using prestack seismic data, *Geophysics*, July 2004, v. 69, p. 978-993. doi: 10.1190/ 1.1778241.

Eiken, O., Ringrose, P., Hermanrud, C., Nazarian, B., Torp, T.A., Høier, L., 2011. Lessons Learned from 14 years of CCS Operations: Sleipner, In Salah and Snøhvit, Energy Procedia, 4, 5541-5548.

Fenghour, A, Wakeman, WA, 1998, The viscosity of carbon dioxide**.** *J. Phys. Chem. Ref. Data*, vol. 27, p. 31-44.

Gassmann, F., 1951, Uber die Elastizitat Poroser Medien, *Vier. Der Natur. Gesellschaftn Zurich*, 96, p.1-23.

Glinsky, M., Asher, B., Hill, R., Flynn, M., Stanley, M., Gunning, J., Thompson, T., Kalifa, J., Mallat, S., White, C., and Renard, D., 2005, Integration of uncertain subsurface information into multiple reservoir simulation models, *The Leading Edge*, October 2005, p. 990 – 999.

Gunning, J., and M. Glinsky, 2007, Detection of reservoir quality using Bayesian seismic inversion, *Geophysics*, vol. 72, no. 3, P. R37 – R49. doi: 10.1190/1.2713043.

Ivandic, M., Yang, C., Lüth, S., Cosma, C., Juhlin, C., 2012. Time-lapse analysis of sparse 3D seismic data from the CO 2 storage pilot site at Ketzin, Germany, Journal of Applied Geophysics, 84, 14-28.

Johnson, J., Nitao J., Knauss K., 2004, Reactive transport modeling of CO_2 storage in saline aquifers to elucidate fundamental processes, trapping mechanisms and sequestration partitioning. In: *Geological Storage of Carbon Dioxide*. Edited by SJ Baines, RH Worden. *Geological Society, London, Special Publications* vol. 223, p. 107-128.

Johnson J., Nitao J., Morris J., 2005, Reactive transport modeling of cap-rock integrity during natural and engineered CO_2 storage. In *Carbon Dioxide Capture for Storage in Deep Geologic Formations*. Edited by D. C. Thomas and S. M. Benson, vol. 2, 787-813.

Law, D., Huang, S., Freitag, N., Perkins, E., Wassmuth, F., Dunbar, B., and Asghari, K., 2004. Theme 3: CO2 Storage Capacity and Distribution Predictions and the Application of Economic Limits, in Wilson, M. and M. Monea (eds), *IEA GHG Weyburn CO_2 Monitoring and Storage Project Summary Report 2000-2004*, Petroleum Technology Research Center, Regina, Canada, 149-210.

Margrave, G., 2003, *Numerical Methods of Exploration Seismology with Algorithms in MATLAB*, Dept. of Geology and Geophysics, University of Calgary, Canada, CREWES Research Consortium.

Metropolis, N., A. Rosenbluth, M. Rosenbluth, A. Teller, and E. Teller (1953), Equation of state calculations by fast computing machines, *J. Chem. Phys*., *1*, no. 6, 1087-1092.

Mosegaard, K., and A. Tarantola, 1995, Monte Carlo sampling of solutions to inverse problems, *Journal of Geophysical Research*, vol. 100, no. B7, p12431-12447.

Nitao, J.J., 1998a, Reference manual for the NUFT flow and transport code, version 2.0: Lawrence Livermore National Laboratory, Livermore, CA, UCRL-MA-130651, 55 p.

Nitao, J.J., 1998b, User's manual for the USNT module of the NUFT Code, Version 2.0 (NP-Phase, NC-component, Thermal): Lawrence Livermore National Laboratory, Livermore, CA, UCRL-MA-130653, 76 p.

PTRC, 2004, *IEA CHG Weyburn* CO_2 *Monitoring & Storage Project Summary Report 2000-2004*, M. Wilson and M. Monea, Eds., Petroleum Technical Research Centre, 283 p.

Quan, Y., and J. Harris, 2008, Stochastic seismic inversion using both waveform and traveltime data and its application to time-lapse monitoring, SEG Expanded Abstracts 27, 1915 (2008); doi:10.1190/1.3059273

Smith, T. M., C. H. Sondergeld, and C. S. Rai, 2003, Gassmann fluid substitutions: A Tutorial, *Geophysics*, Vol. 68, No. 2, p. 430 - 440.

Span, R, Wagner, W, 1996, A new equation of state for carbon dioxide covering the fluid region from the triple-point temperature to 1100 K at pressure up to 800 MPa**.** *J. Phys. Chem. Ref. Data*, vol. 25, p. 1509-1596.

Wilson, M. and M. Monea (eds), 2004, *IEA GHG Weyburn* CO_2 *Monitoring and Storage Project Summary Report 2000-2004*, Petroleum Technology Research Center, Regina, Canada, 283 p.

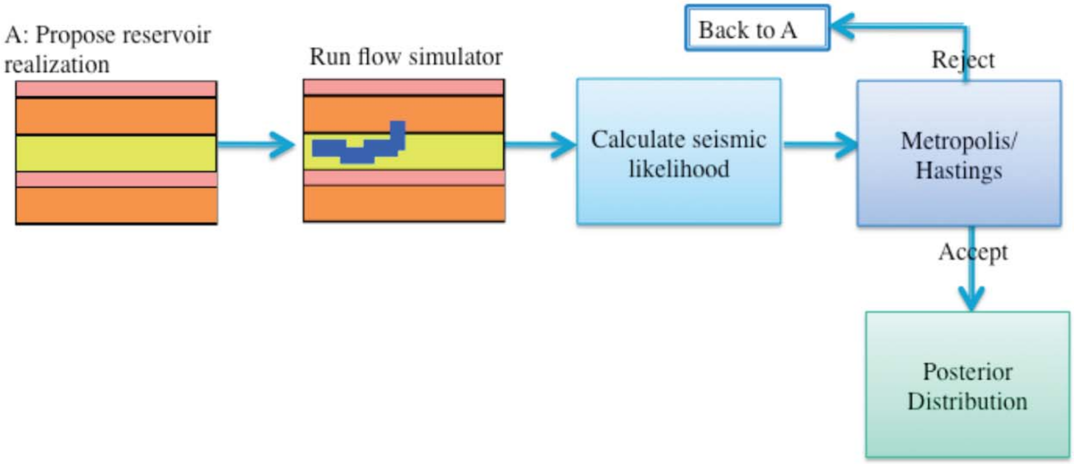
Back to A
A: Propose reservoir realization
Run flow simulator
Calculate seismic likelihood
Metropolis/ Hastings
Reject
Accept
Posterior Distribution

Figure 1. Flow diagram for the first inversion step using seismic data. Note that the process will use two or more seismic data sets simultaneously.

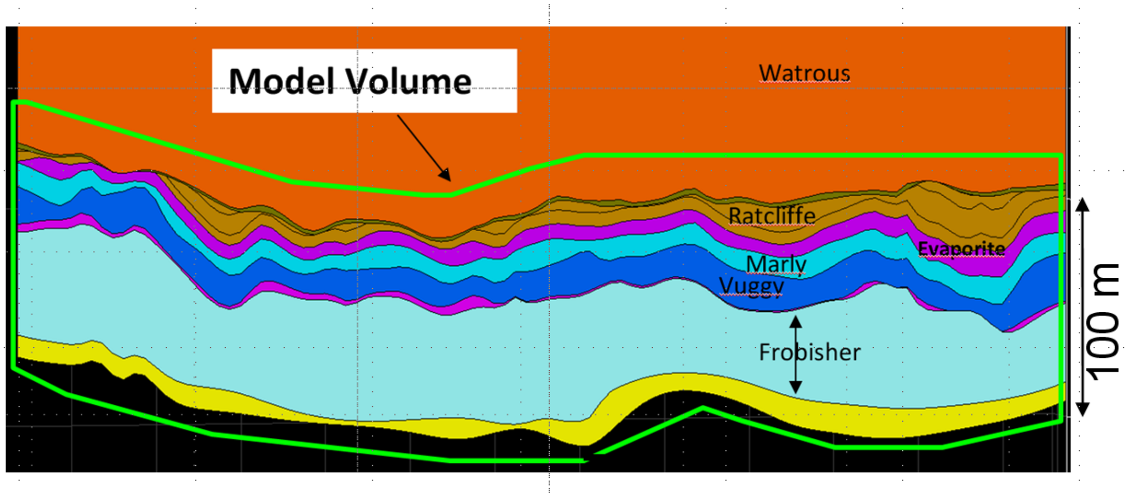
Model Volume
Watrous
Ratcliffe
Evaporite
Marly
Vuggy
Frobisher
100 m

Figure 2. Geological model used as the basis for inversion.

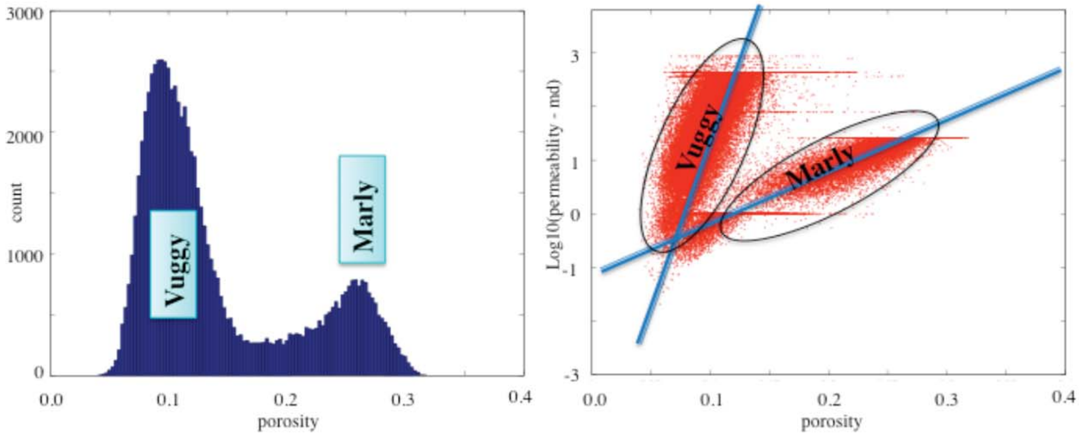

Figure 3. Left panel, histogram of porosity recovered from Cenovus' model. Right panel, cross-plot of porosity versus log10(permeability – milli-darcies).

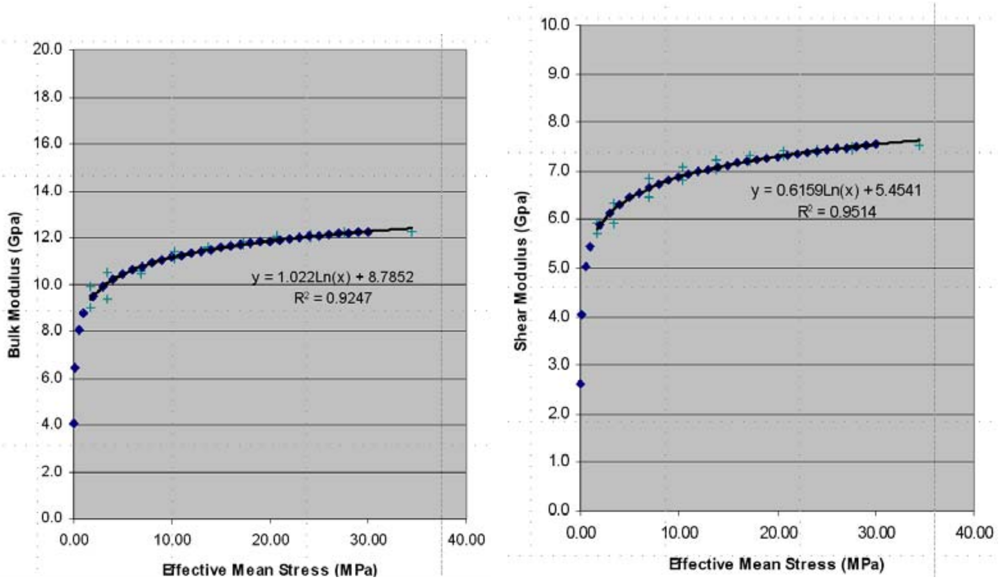

Figure 4. Pressure dependence of bulk and shear modulus for the Midale Marly unit utilized in the inversion. Data points are from Brown (2002).

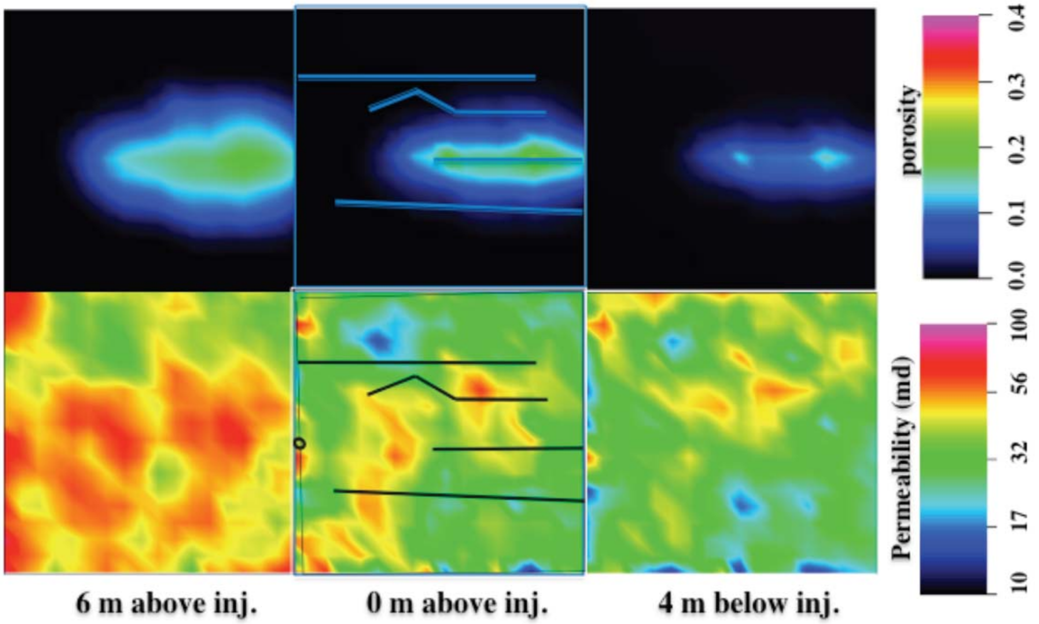

Figure 5. The top row of images shows the CO2 distribution calculated assuming the permeability distribution in the bottom row of images. The image planes are horizontal and located at the elevation of the CO2 injector, 6m above the injector and 4 m below the injector. The CO2 saturation color bar is at the top right corner of the image. The permeabilities are in millidarcies (bottom right color bar).

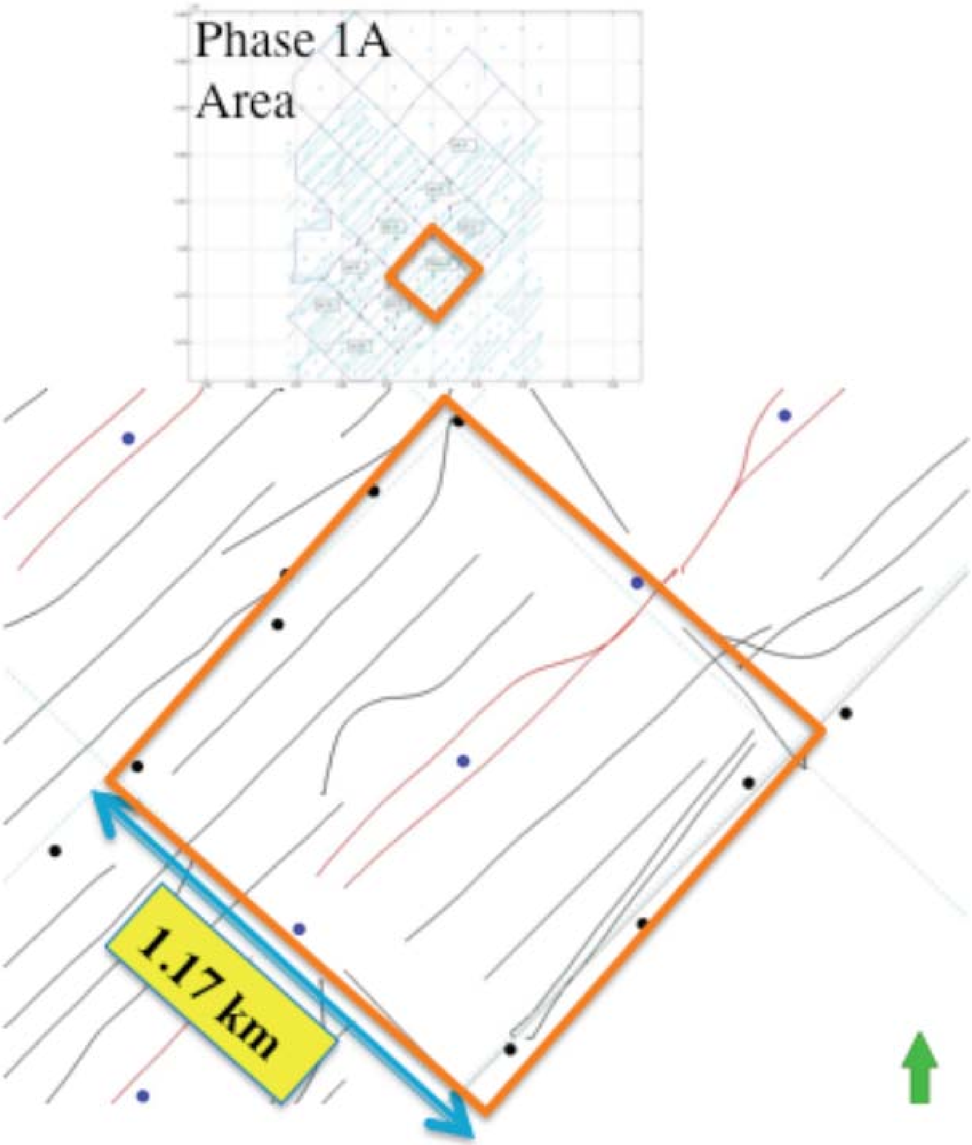

Figure 6. Shows the Phase 1A pattern considered by our study. The blue circles represent vertical water injection wells. The black circles and lines represent vertical and horizontal production wells, respectively. The red lines represent CO2 injection wells.

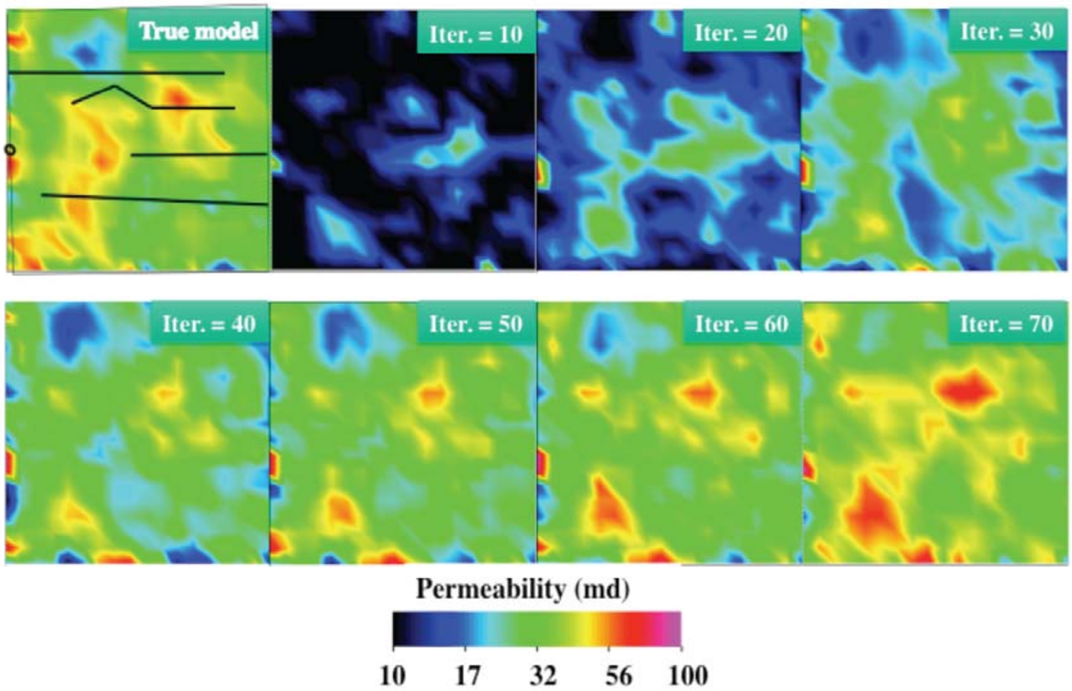

Figure 7a. The top left image shows the true permeability distribution and the locations of the CO2 injector, oil producers and water injectors. The CO2 injector is coplanar with the horizontal image plane shown. The remaining images show the recovered permeabilities as a function of MCMC iteration.

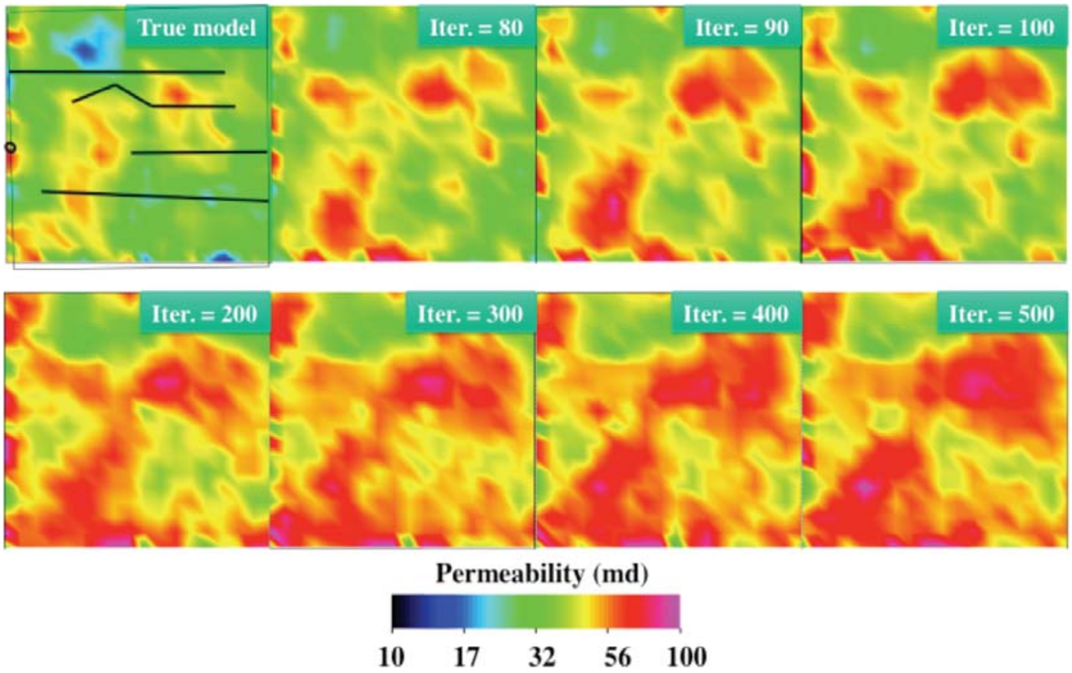

Figure 7b. The top left image shows the true permeability distribution and the locations of the CO2 injector, oil producers and water injectors. The CO2 injector is coplanar with the image plane shown. The remaining images show the recovered permeabilities as a function of MCMC iteration.

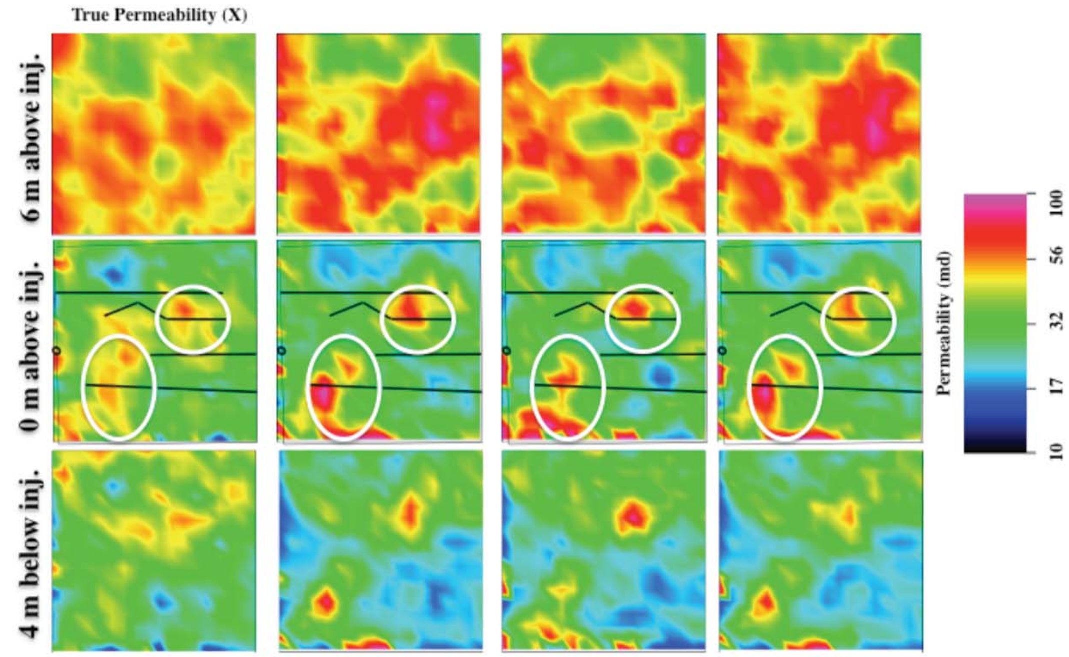

Figure 8. The left column of images shows horizontal slices through the true permeability model. The next three columns show recovered permeability distributions that best fit the synthetic seismic data.

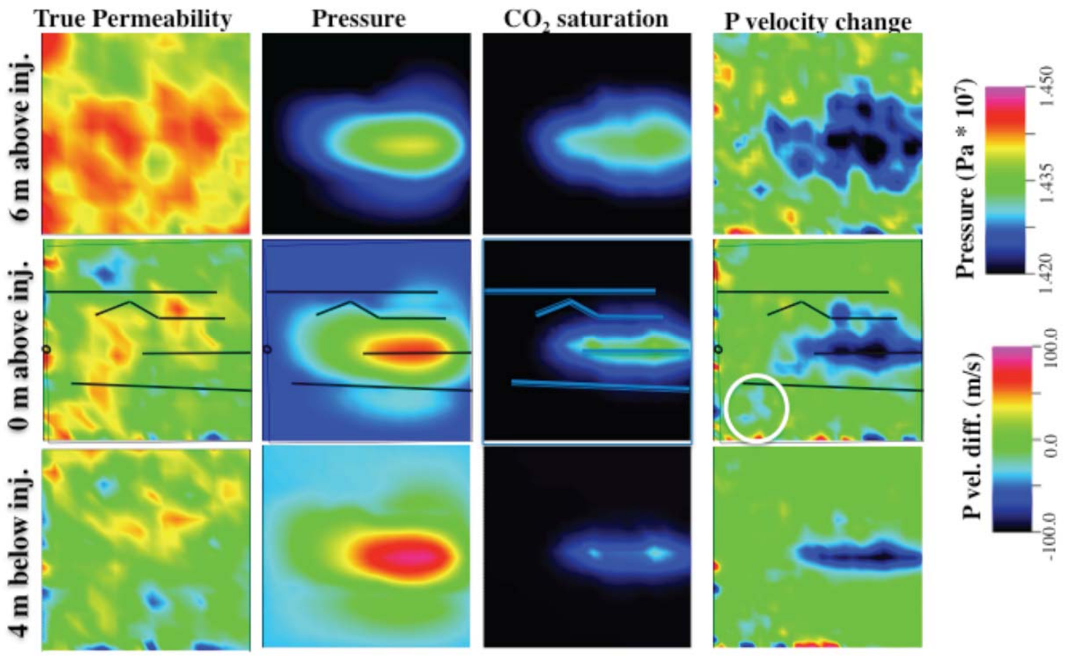

Figure 9. The left column of images shows the "true" permeability model. The second and third image columns show the calculated pressure and CO2 saturation that develop after 1.3 years of CO2 injection. The fourth image column shows changes in P velocity (V1 – V2) predicted, where V1 = velocity at ambient pressure and no CO2, and V2 = velocity at injection pressures and CO2 saturations. The velocity changes within the white ellipse region are likely caused by pressure fluctuations created by the injection/extraction process.

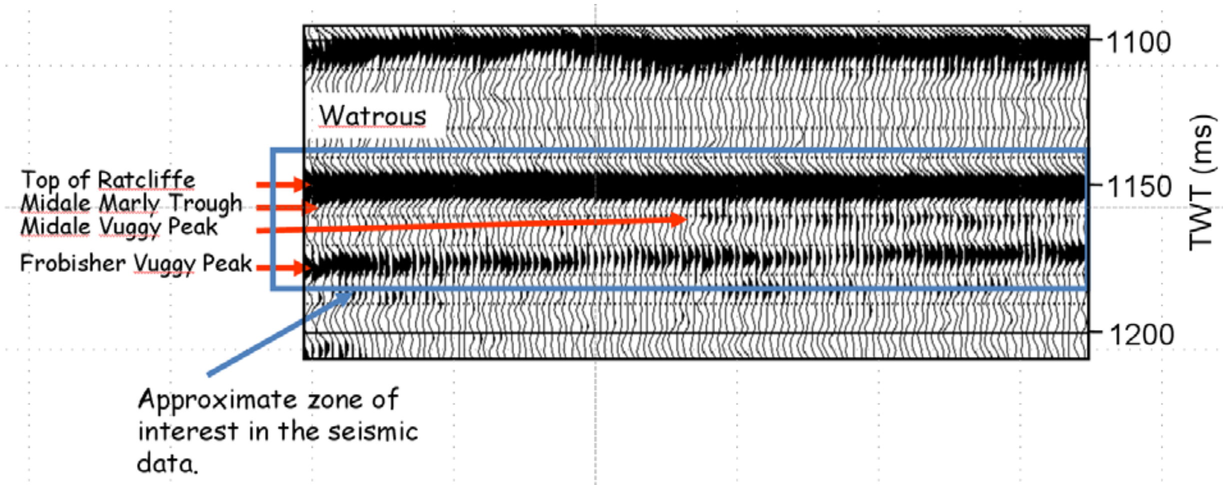

Figure 10. Example of the observed seismic data for the reservoir zone.

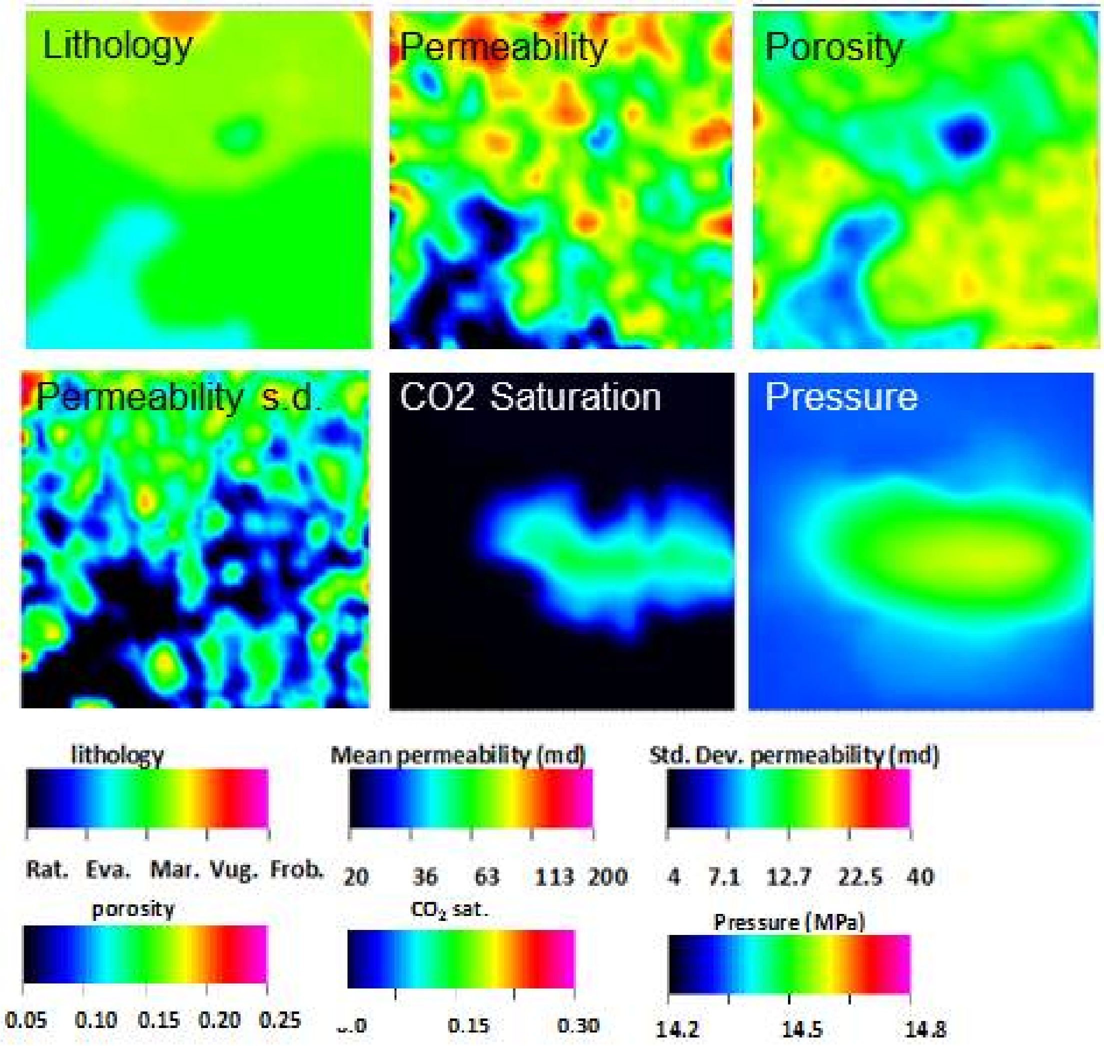
Lithology
Permeability
Porosity
Permeability s.d.
CO2 Saturation
Pressure
lithology
Rat. Eva. Mar. Vug. Frob.
Mean permeability (md)
20 36 63 113 200
Std. Dev. permeability (md)
4 7.1 12.7 22.5 40
porosity
0.05 0.10 0.15 0.20 0.25
CO_2 sat.
0 0.15 0.30
Pressure (MPa)
14.2 14.5 14.8

Figure 11. Model from iteration 5751. The horizontal slices show the lithologies, permeability, porosity, permeability standard deviation, along with the corresponding CO_2 saturations and pore pressures. The horizontal slices are located 4 m above the location of the CO_2 injector. Note that the slice is located mostly within the Marly unit.

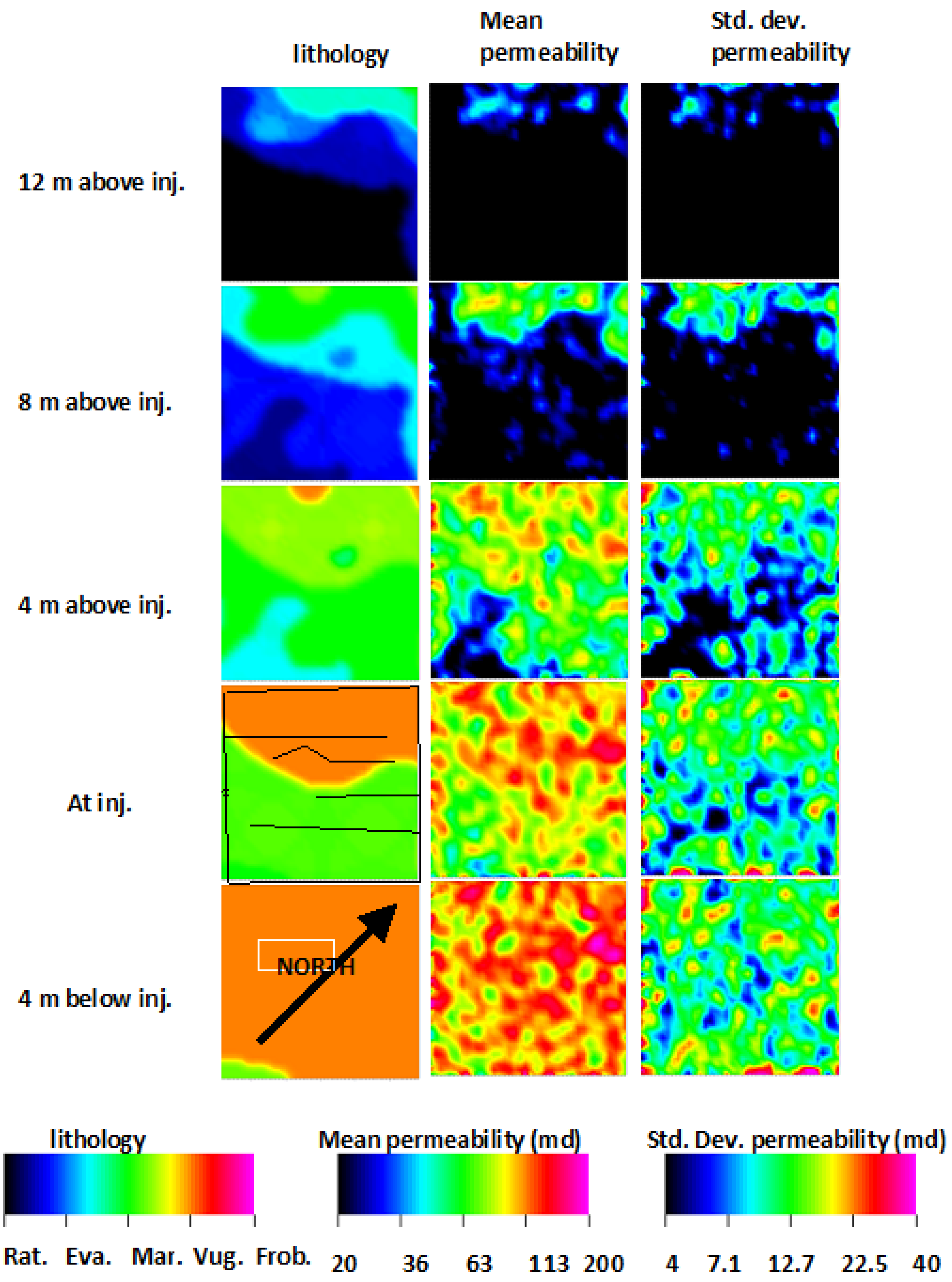

Figure 12. Lithology, mean and standard deviation for all the permeability models with iteration number greater than 5700. The permeabilities are shown in milli-Darcy (mD), on a logarithmic scale. The apparent gradations in lithology (1st column) are an artifact of the smoothness filter used by the visualization software.

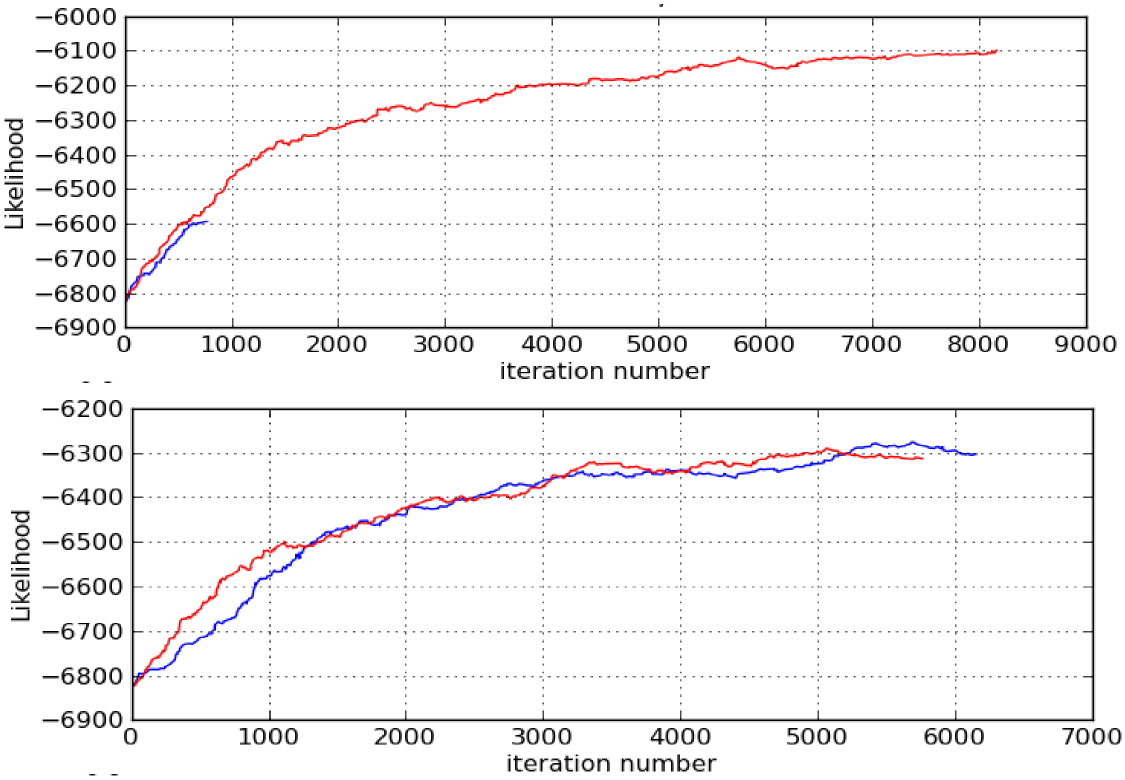

Figure 13 The plots show likelihood value as a function of iteration for two permeability inversion runs that used different step sizes. The step size associated with the top plot was about ten times larger (on average) than the step size for the bottom plot. The top plot indicates that a solution with better likelihood (closer to 0) has been found using the larger step size. Likelihood is a measure of the similarity between the predicted and observed seismic waveforms. Note that a stable value is achieved after about 5700 iterations (top plot) and 5000 iterations (bottom plot).

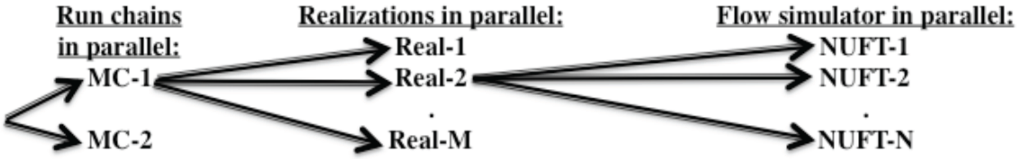
Run chains in parallel:
MC-1
MC-2
Realizations in parallel:
Real-1
Real-2
.
Real-M
Flow simulator in parallel:
NUFT-1
NUFT-2
.
NUFT-N

Figure 14. Shows schematic implementation of the nested, parallel-thread approaches used to optimize run-time performance.

Appendix A: The inversion algorithm

Details are presented here regarding the inversion algorithm described in the main text and schematically illustrated in Figure 1.

1. Propose reservoir model realizations

Reservoir model realizations are populated with porosity/permeability data based on prior knowledge of the relationship between lithology and porosity/permeability for the specific depositional setting. Reservoir model proposals are generated by randomly perturbing the existing Cenovus reservoir model. Random perturbations of the permeabilities and porosities are generated as governed by the a priori distributions shown in Figure 3. This is done as follows:

1) Read in Cenovus's geologic model
2) Initialize layer values. For each lithologic layer:
    - 2a) Read starting model containing lithologies, and initial porosities, and permeabilities.
    - 2b) Calculate average value of porosity and permeability
    - 2c) Identify grid nodes associated with each layer
    - 2d) Assign average value of porosity and permeability to each node
3) Generate realization of porosity and permeability fields. For each lithologic layer:
    - 3a) Choose at random ~ 5 - 10% of nodes to change porosity/permeability. For each node to be changed:
        - 3a.1) Randomly choose a value of porosity probability (chosenProb) *(use the probability ranges implied by the Fig. 3 histogram).*
        - 3a.2) List possible porosity values that have probability > chosenProb
        - 3a.3) Choose random porosity value from the 3a.2 list
        - 3a.4) List possible permeability values for the porosity chosen in 3a.3 *(use the porosity/permeability correlations in Fig. 3, bottom row)*
        - 3a.5) Choose a random permeability from the list of possible values, (assuming a lognormal distribution).
        - 3a.6) Assign new porosity and permeability values to grid node

These realizations are used by the flow simulator.

2. Flow simulation

The Nonisothermal Unsaturated-Saturated Flow and Transport code (NUFT) is used for reservoir-scale multiphase flow and reactive transport simulations. NUFT is used to simulate flow within the reservoir caused by injection/extraction of CO_2, H_2O and oil. The NUFT code is a highly flexible software package for modeling multiphase, multi-component heat and mass flow and reactive transport in unsaturated and saturated porous media (Nitao, 1998). An integrated finite-difference spatial discretization method along with implicit time-integration scheme is used to solve mass and energy balance equations in flow and reactive transport models. At each time step the resulting nonlinear equations are solved by the Newton-Raphson method. The NUFT code has been used for applications such as geologic disposal of nuclear waste, CO_2 sequestration and storage, groundwater remediation, and subsurface hydrocarbon production (e.g., Buscheck et al., 2003; Johnson et al., 2004, 2005).

For multiphase flow modeling of the reservoir, the top and bottom boundaries are kept impermeable and hydrostatic pressure conditions are assigned along the lateral boundary. Vertical and horizontal production wells, and horizontal injection wells are included in the model. CO_2 is injected under supercritical conditions. Due to the presence of water, oil and supercritical CO_2, three-phase flow conditions are considered and equilibrium conditions are assumed for component partitioning among three phases. The equation-of-state and viscosity of CO_2 under supercritical conditions are obtained based on the empirical equations developed by Span and Wagner (1996) and Fenghour and Wakeman (1998), respectively. The water and oil properties (pressure, volume, temperature) are computed using the empirical formulas that can be found in most of textbooks on reservoir modeling (e.g. Chen et al., 2006). The injection-induced reservoir pressure perturbations along with CO_2 plume distributions are predicted by the reservoir flow model.

3. Calculate seismic likelihood

The next step is to calculate zero-offset seismograms using the information produced by the CO_2 flow simulator (NUFT). The resultant seismograms can then be compared to the observed seismic data to determine the a posterior likelihood. The components of this process are:

1) Calculate elastic properties using Gassmann's relations for current reservoir conditions
2) Calculate corresponding seismic reflectivity
3) Calculate zero-offset (1D) seismograms
4) Compare the predicted and observed seismograms to compute the likelihood that the predicted waveforms come from the "true" model.

3.1 Calculate elastic parameters

As the fluid saturations, temperature and pressure conditions change during CO_2 injection, the reservoir's elastic parameters (bulk and shear moduli) and density change. Consequently, seismic velocities and impedances change resulting in seismic reflectivity changes within the reservoir. Fluid substitution techniques are used to predict these changes for a range of fluid scenarios using Gassmann's equation (Gassmann, 1951) as described in Smith et al. (2003). In this manner, the elastic moduli and associated seismic velocities of a fluid-saturated rock are obtained from the rock porosity, elastic moduli of the porous dry rock frame and the constituent mineral matrix, and the bulk moduli and densities of the pore fluids.

The fluid substitution modeling invoked here follows the procedure described in Smith et al. (2003), but introduces modifications where some derived quantities are replaced with quantities measured on core samples from the Weyburn field. The algorithm consists of the following:

1. Obtain mineral matrix bulk modulus (K_o) based on core measurements (see Table 1).
2. Calculate fluid bulk modulus (K_{fl}) and density based on saturations, bulk moduli and densities of constituent fluids for appropriate pressure, temperature conditions. Obtain individual bulk moduli from equations of state for each fluid. Use equation 3 (below).
3. Obtain dry porous rock framework bulk modulus (K^*) for appropriate pressure, temperature conditions (e.g., Figure 4).
4. Calculate moduli for saturated rock using the Gassmann equation. Use equation 4 (below) and appropriate porosity value (ϕ).
5. Calculate Vp, Vs for saturated rock using the moduli from step 4. Use equations 5-7 (below).

The equation used to calculate the composite fluid modulus is:

$$\begin{aligned}
&K_{fl} = \frac{S_w}{K_w} + \frac{S_{oil}}{K_{oil}} + \frac{S_{co2}}{K_{co2}} \\
&K_w = brine\_\mathrm{mod}ulus \\
&K_{oil} = oil\_\mathrm{mod}ulus \\
&K_{co2} = co2\_\mathrm{mod}ulus \qquad (3) \\
&S_w = brine\_saturation \\
&S_{oil} = oil\_saturation \\
&S_{co2} = co2\_saturation
\end{aligned}$$

The brine modulus (K_w) is calculated using the approach of Batzle and Wang (1992) equations 27 - 29. They use a combination of thermodynamic relationships, empirical trends and data to develop simplified relationships that produce estimates of realistic fluid properties in rock models.

The oil modulus (K_{oil}) and CO_2 modulus (K_{co2}) is computed using the compressibilities computed by the NUFT simulator.

Gassmann's equation used to calculate saturated rock bulk moduli (K_{inj}) is:

$$K_{inj} = K^* + \frac{(1 - \frac{K^*}{K_0})^2}{\frac{\phi}{K_{fl}} + \frac{1-\phi}{K_0} + \frac{K^*}{K_0^2}} \qquad (4)$$

Once (K_{inj}) is calculated, we are ready to calculate the P and S seismic velocities (V_p ,V_s):

$$V_p = \sqrt{\frac{K_{inj} + \frac{4}{3} G_{init}}{\rho_b}} \qquad (5)$$

where ρ_b is the bulk density under initial (pre-injection) conditions and,

$$G_{init} = \rho_b V_{s,core}^2 \tag{6}$$

where $V_{s,core}$ is the shear velocity measured on dry rock core (e.g., see Figure 4).

3.2 Calculate synthetic waveforms

1D seismograms are calculated using the approach described by Margrave (2003). Use of a 1-D model is considered appropriate because the seismic data we use has been migrated and the layering is approximately horizontal. Margrave's approach constructs the reflection response of a 1D medium to a unit impulse. The impulse response only considers primary reflections and ignores multiple reflections. This impulse response is then convolved with an appropriate wavelet that simulates the effects of the seismic source. The resulting waveform is the synthetic 1D seismogram that will be compared with the observed 1D seismograms.

Reflection coefficients (*R;* or reflectivity) determine the amount of reflected signal generated at each layer interface and, collectively form the impulse response along a vertical line of nodes. In equation 7, R is the reflection coefficient between two layers having seismic impedances I_1 (top layer) and I_2 (bottom layer). Seismic impedance is a function of seismic velocity and bulk density as shown in equation 8.

$$R = (I_2 - I_1)/(I_2 + I_1) \tag{7}$$

$$I = V\rho_b \tag{8}$$

A wavelet derived from the observed seismic data is then convolved with the reflectivity series to produce synthetic 1D seismograms.

3.3 Calculate likelihood function

We now describe Metropolis-Hastings algorithm, the importance sampling algorithm we use to decide whether the proposed model should be accepted or rejected. The likelihood $L(\underline{x})$ is a measure of the degree of fit between the data predicted (i.e., the calculated seismograms described previously) assuming model $\underline{x}$ and the observed data (fully processed, filed data derived seismograms), and *k* is a normalizing constant. In our approach, we use a likelihood function of the form:

$$L(\underline{x}) = k \exp\left(-\frac{1}{n} \sum_{i=1}^{N} \frac{\left| d(\underline{x})_{pred,i} - d_{0,i} \right|^n}{\sigma_i^n} \right) \tag{10}$$

where N is the number of data points, $d(\underline{x})_{pred,i}$ is the predicted data for a given model $\underline{x}$, $d_{0,i}$ is the vector of observed measurements, σ_i is the estimated data uncertainty, and $n \geq 1$. We note that most deterministic inversions also use the term in parentheses as a measure of goodness of fit.

The decision to accept or reject a proposed model is made on the basis of likelihood comparisons. Suppose that the current model of the Markov chain is $\underline{x}^{(T)}$ and that a move to an adjacent model $\underline{x}^{(T+1)}$ is proposed. If these transitions were always accepted, then our MCMC method would be sampling from the prior distribution $\rho(\underline{x})$, i.e., the observed data $\underline{d}_0$ would not influence the search.

$$\begin{aligned} &L(\underline{x}^{(T+1)}) > L(\underline{x}^{(T)}) : P_{accept} = 1 \\ &L(\underline{x}^{(T+1)}) \leq L(\underline{x}^{(T)}) : P_{accept} = L(\underline{x}^{(T+1)}) / L(\underline{x}^{(T)}) \end{aligned} \qquad (11)$$

Instead, suppose that the decision to accept the proposed transition is made as follows (see eq. 11). When the likelihood of the proposed model $L(\underline{x}^{(T+1)})$ is equal to or larger than that of the current model $L(\underline{x}^{(T)})$, the proposed transition is always accepted. If $L(\underline{x}^{(T+1)}) < L(\underline{x}^{(T)})$ but the two values are close to each other, the probability of acceptance is still around 1.0. For example, suppose that $L(\underline{x}^{(T)})$ = 10 and $L(\underline{x}^{(T+1)})$ = 9. In this case, the probability of acceptance (P_{accept}) will be 9/10 or 0.9. We then generate a uniformly random number *RN* in the range 0 to 1.0. When $P_{accept} > RN$, the transition to model $\underline{x}^{(T+1)}$ is accepted. Note that there is a high probability of accepting $\underline{x}^{(T+1)}$ because the odds are very high that $P_{accept} > RN$. Next, let's suppose that the model $\underline{x}^{(T+1)}$ is much less consistent with the data such that $L(\underline{x}^{(T+1)})$ = 0.9. In this case, P_{accept} is 0.09, the odds that $P_{accept} > RN$ are much smaller and thus, the odds of accepting the transition are a lot smaller. However, even when $L(\underline{x}^{(T+1)}) << L(\underline{x}^{(T)})$, P_{accept} is not zero. Thus, this randomized rule allows a transition to a less likely model such that the process will move out of a local extremum. Theoretically, it will never get trapped in a region of locally high likelihood as long as the likelihood of the proposed model is greater than 0.0. Then, the randomized acceptance rule guarantees that the probability of accepting this transition will always be greater than 0.0.

Metropolis et al. (1953) proved that the samples generated through this process has a limiting distribution that is proportional to the desired posterior distribution $\mathrm{P}(\underline{x} | \underline{d})$ -- the probability of model $\underline{x}$ being the true model of nature given that $\underline{d}$ has been measured. As a result of the randomized rule, the search tends to hover in regions of space X containing models that better fit the prior information and seismic measurements. Because of this, space X is traversed more efficiently than with traditional Monte Carlo techniques.

If the decision is to accept model $\underline{x}^{(T+1)}$, it becomes a part of the posterior distribution, and the next proposal ($\underline{x}^{(T+2)}$) will be generated as a random perturbation about $\underline{x}^{(T+1)}$. Alternatively, if the decision is made to reject $\underline{x}^{(T+1)}$, a copy of $\underline{x}^{(T)}$ is added to posterior distribution, and the next proposal ($\underline{x}^{(T+2)}$) will be generated as a random perturbation about $\underline{x}^{(T)}$. The net result of this approach is that solutions are sampled at a rate proportional to their consistency with available data.

This is a key strength of our MCMC approach. Models that are most consistent with available data observations are sampled most often, while models that are incompatible with either prior information and/or observations are rarely sampled. As a result, the frequency of models in the posterior distribution $\mathrm{P}(\underline{x}|\,\underline{d})$ can be used to determine the probability that a given model is the best explanation for the available data. It can also be used to objectively rank alternative models that are consistent with the data.

3.4 Compare predicted and observed seismic waveforms

Comparison of predicted and observed waveforms is required in order to calculate the likelihood function, specifically the numerator term in eq. 10. The algorithm we have developed follows (*comments shown in italics*).

1) Trim the observed waveforms (W_{obs}) to only include the part that corresponds to the reservoir box.
2) Scale the amplitudes of the predicted waveforms (W_{pred}) and W_{obs}. Scale such that the maximum value of each is set to 1.0. *This is done because the W_{pred} and W_{obs} data have arbitrary units and thus, need to be amplitude-matched.*
3) Cross-correlate W_{pred} and W_{obs} to determine the delay-time.
4) Time-shift W_{pred} so that it aligns with W_{obs}.
5) Compute the difference in amplitude for each waveform time-step and sum the absolute value of the differences. This corresponds to the operation shown on the right hand of eq. 10.

Geological Unit	Bulk Modulus (GPa)	Shear Modulus (GPa)	Density (kg/m^3)
Watrous	??	??	??
Ratcliffe	76.3	33.0	2740
Midale Evaporite	73.7	39.1	2803
Midale Marly	79.4	37.7	2824
Midale Vuggy	76.3	33.0	2740
Frobisher Marly	80.9	39.5	2838
Frobisher Vuggy	76.3	33.0	2740

Table 1. Mineral matrix bulk properties used for geologic units in calculation of the seismic response. Bulk properties were determined using the mineral fractions in Table 3.6 of Law et al. (2004) and the moduli values in Smith et al. (2003).